AFM's path to atomic resolution

by Franz J. Giessibl

We review progress in improving the spatial resolution of atomic force microscopy (AFM) under vacuum. After an introduction to the basic imaging principle and a conceptual comparison to scanning tunneling microscopy (STM), we outline the main challenges of AFM as well as the solutions that have evolved in the first 20 years of its existence. Some crucial steps along AFM's path toward higher resolution are discussed, followed by an outlook on current and future applications.

AFM, invented[1] and introduced[2] in 1986, can be viewed as a mechanical profiling technique that generates three-dimensional maps of surfaces by scanning a sharp probe attached to a cantilever over a surface. The forces that act between the tip of the cantilever and the sample are used to control the vertical distance. AFM's potential to reach atomic resolution was foreseen in the original scientific publication[2] but, for a long time, the spatial resolution of AFM was inferior to the resolution capability of its parent technique, STM.

The resolution limits of STM and AFM are given by the structural properties of the atomic wavefunctions of the probe tip and the sample. STM is sensitive to the most loosely bonded electrons with an energy at the Fermi level, while AFM responds to all electrons, including core electrons. Because electrons at the Fermi level are spatially less confined than core electrons, in theory AFM should be able to achieve even greater spatial resolution than STM. Today, experimental evidence is emerging where, in simultaneous AFM/STM studies, AFM images reveal even finer structural details than simultaneously recorded STM images.

The experimental advances that made high-resolution AFM possible began with the introduction of frequency-modulation AFM (FM-AFM). Here, the cantilever oscillates at a fixed amplitude and frequency is used as a feedback signal. Early implementations of FM-AFM used Si cantilevers with a typical spring constant of 10 N/m, which oscillate with an amplitude on the order of 10 nm. The spatial resolution was increased by the introduction of quartz cantilevers with a

Experimentalphysik VI, EKM,
Institute of Physics, Augsburg University,
86135 Augsburg, Germany
E-mail: franz.giessibl@physik.uni-augsburg.de

stiffness on the order of 1 kN/m, allowing the use of subnanometer amplitudes. The direct evaluation of higher harmonics in the cantilever motion has enabled a further increase in spatial resolution.

Because AFM can image insulators as well as conductors, it is now a powerful complement to STM for atomically resolved surface studies. Immediate applications of high-resolution AFM have been demonstrated in vacuum studies relating to materials science, surface physics, and surface chemistry. Some of the techniques developed for ultrahigh-vacuum AFM may be applicable for increasing AFM resolution in the ambient or liquid environments that are necessary for studying biological or technological specimens.

Principles of AFM operation

AFM[1,2] can be viewed as an extension of the toddler's way of 'grasping' the world by touching and feeling, as indicated in Fig. 1 of Binnig and Rohrer's article[3], where a finger profiles an atomic surface. Likewise, one could argue that stylus profilometry is a predecessor of AFM. However, AFM and stylus profilometry have as much in common as a candle and a laser. Both generate light and, even though candles are masterpieces of engineering[4], the laser is a much more advanced technological device requiring a detailed knowledge of modern quantum mechanics[5]. While stylus profilometry is an extension of human capabilities that have been known for ages and works by classical mechanics, AFM requires a detailed understanding of the physics of chemical bonding forces and the technological prowess to measure forces that are several orders of magnitude smaller than the forces acting in profilometry.

Only the spectacular spatial resolution of STM could trigger the hope that the force acting between an STM tip and a sample might lead to AFM capable of true atomic resolution. Established in 1981, the STM was the first instrument to allow surface imaging with atomic resolution in real space[6,7]. The atomic imaging of the 7×7 reconstruction of Si (111) by STM in 1983[8] later helped to solve one of the most intriguing problems of surface science at that time and establish the dimer-adatom-stacking fault model of Takayanagi *et al.*[9]. The atomic resolution capability of STM provided immediate evidence for the enormous value of this instrument as a tool for surface scientists.

STM can only be used on conductive surfaces. Given that many surfaces of technological interest are conducting or at least semiconducting, this may not seem a severe shortcoming. One might think that an STM should be capable of mapping a metallic surface under ambient conditions. However, this is not feasible because the pervasive layer of oxides and other contaminants that occurs at ambient conditions prevents stable tunneling conditions. Electrical conductivity is a necessary but not sufficient condition for a surface to be imaged by STM with atomic resolution, because the surface needs to be extremely clean on an atomic level. Except for a few extremely inert surfaces such as graphite, atomic resolution is only possible in an ultrahigh vacuum with a pressure on the order of 10^{-8} Pa and special surface preparation.

The invention of the AFM by Binnig[1], and its introduction by Binnig, Quate, and Gerber[2], opened up the possibility of obtaining true atomic resolution on conductors and insulators. Indeed, it took only a short time after the AFM's invention before apparent atomic resolution on conductors[10] and insulators[11-13] was obtained. While these early results reproduced the periodic lattice spacings of the studied samples, single defects or step edges were not observed. Also, the forces that acted between tip and sample were often orders of magnitudes larger than the forces that a tip with a single front atom was expected to be able to sustain. It was commonly assumed, therefore, that many tip atoms interacted with the surface at the same time in these early experiments. The difference between apparent and true atomic resolution of a tip with many atomic contacts can be illustrated by a macroscopic example. When profiling an egg crate with a single egg, its trajectory would represent the overall periodicity of the crate as well as each dented hump or a hole. However, when profiling one egg crate with another egg crate, again its periodicity would be retained but holes or dented humps would pass undetected. A similar effect can occur when an AFM tip probes a surface. As long as single defects, steps, or other singularities are not observed, clear proof for true atomic resolution is not established.

Even though atomic resolution was hardly ever achieved in the initial AFM experiments, the technique was readily accepted and found many technological and scientific applications. The installed base of AFMs rapidly outnumbered their STM counterparts. A recent survey[14] of the ten most highly cited publications in *Phys. Rev. Lett.* ranks the original AFM publication[2] at number four (4251 citations as of March 11, 2005 according to ISI) – in good company with

other breakthroughs in theoretical and experimental physics that have shaped our scientific life. Most of these citations refer to AFM where the spatial resolution is 'only' in the nanometer range, but the large number shows the vast range of AFM applications. In spite of the rapid growth of AFM usage, matching and even exceeding the spatial resolution of its parent, STM, had to wait for new developments.

Challenges in achieving atomic resolution

The technological foundations for achieving STM with atomic resolution (theory of electron tunneling, mechanical actuation with picometer precision, vacuum technology, surface and tip preparation, vibration isolation, etc.) were probably available a few decades before 1981, but it took the bold approach by Binnig, Rohrer, Gerber, and Weibel to pursue atomic resolution in real space. Binnig and Rohrer were rewarded with the 1986 Nobel Prize in Physics (together with Ernst Ruska, inventor of electron microscopy).

The challenges in gaining AFM with true atomic resolution are even more daunting than the hurdles that troubled STM. Fig. 1a shows a schematic view of a sharp tip for STM or AFM close to a crystalline sample, and Fig. 1b is a plot of the tunneling current and forces between tip and sample. When tip and sample are conductive and a bias voltage is applied between them, a tunneling current can flow. The red curve in Fig. 1b shows the distance dependence of the tunneling current I_t. The exponential decay of I_t with increasing distance at a rate of approximately one order of magnitude per 100 pm is the key physical characteristic that makes atomic-resolution STM possible. Because of its strong decay rate, the tunneling current is spatially confined to the front atom of the tip and flows mainly to the sample atom next to it (indicated by red circles in Fig. 1a). A second helpful property of the tunneling current is its monotonic distance

dependence. It is easy to build a feedback mechanism that keeps the tip at a constant distance: if the actual tunneling current is larger than the setpoint, the feedback needs to withdraw the tip and vice versa.

In contrast, the tip-sample force F_{ts} does not share the helpful characteristics of the tunneling current. First, F_{ts} is composed of long-range background forces, depicted in light-blue in Fig. 1b and originating from the atoms colored light-blue in Fig. 1a, as well as a short-range component, depicted in blue in Fig. 1b and confined to the atoms printed in blue in Fig. 1a. Because the short-range force is not monotonic, it is difficult to design a feedback loop that controls distance by using the force. A central task to perfect AFM is, therefore, the isolation of the front atom's force contribution and the creation of a linear feedback signal from it.

Even if it was possible to isolate the short-range force, a more basic problem needs to be solved first: how to measure small forces. For example, commonly known force meters, such as precise scales, are delicate and expensive instruments and even top models rarely exceed a mass resolution of 100 µg, corresponding to a force resolution of 1 µN. In addition, high-precision scales take ~1 s to acquire a weight measurement, so the bandwidth is only 1 Hz. The force meters in AFM, in contrast, require a force resolution of at least 1 nN at a typical bandwidth of 1 kHz.

Most force meters determine the deflection q' of a spring with given spring constant k that is subject to a force F with $F = q'/k$. Measuring small spring deflections is subject to thermal drift and other noise factors, resulting in a finite deflection measurement accuracy $\delta q'$. The force resolution is thus given by $\delta F = \delta q'/k$, and soft cantilevers provide less noise in the force measurement.

In contact-mode AFM, where the tip feels small repulsive forces from the sample surface, the cantilever should be softer than the bonds between surface atoms (estimated at ~10 N/m) otherwise the sample deforms more than the cantilever[15]. Because of noise and stability considerations, spring constants below 1 N/m or so have been chosen for AFM in contact mode. However, atomic forces are usually attractive in the distance regime that is best suited for atomic-resolution imaging (approximately a few hundred picometers before making contact), and soft cantilevers suffer from a 'jump-to-contact' phenomenon, i.e. when approaching the surface, the cantilever snaps toward the surface ending in an uncontrolled landing. While true atomic
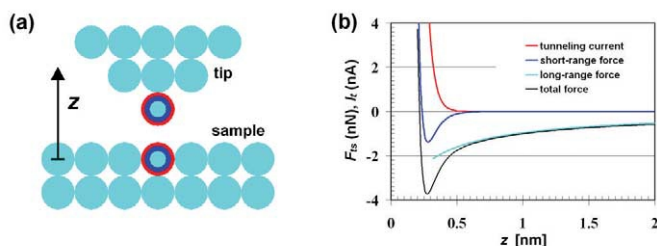

Fig. 1 (a) Schematic of tip and sample in STM or AFM. The diameter of a metal atom is typically 0.3 nm. (b) Qualitative distance dependence of tunneling current, long-, and short-range forces. Tunneling current increases monotonically with decreasing distance, while total force reaches a minimum and increases for distances below the bond length.

resolution by contact-mode AFM has been demonstrated on chemically inert samples[16,17], this method is not feasible for imaging chemically reactive surfaces where strong, attractive short-range forces act. Long-range attractive forces are compensated in these experiments by pulling at the cantilever (negative loading force) after jump-to-contact[16] or by immersing cantilever and sample in water to reduce the van der Waals attraction[17]. Howald *et al.*[18] partially solved the reactivity problem by passivating the reactive Si tip with a thin layer of polytetrafluoroethylene (teflon). The unit cell of Si(111)-(7×7) was resolved, but atomic resolution was not reported with this method of tip passivation.

In summary, AFM shares challenges already known in STM and uses many of its design features (actuators, vibration isolation, etc.), but nature has posed four extra problems for atomic-resolution AFM: (i) jump-to-contact; (ii) nonmonotonic short-range forces; (iii) strong, long-range background forces; and (iv) instrumental noise in force measurements.

Frequency-modulation AFM

Dynamic AFM modes[19-21] help to alleviate two of the four major AFM challenges. Jump-to-contact can be prevented by oscillating the cantilever at a large enough amplitude A such that the withdrawing force on the cantilever given by $k \times A$ is larger than the maximal attractive force[22]. Because the noise in cantilever deflection measurements has a component that varies in intensity inversely with frequency ($1/f$ noise), dynamic AFM modes are less subject to noise than quasistatic operating modes. Nonmonotonic interactions and strong, long-range contributions are still present.

In amplitude-modulation AFM[19], the cantilever is driven at a constant frequency and the vibration amplitude is a measure of the tip-sample interaction. In 1991, Albrecht *et al.*[20] showed that FM-AFM offers even less noise at larger bandwidth than amplitude-modulation AFM. In FM-AFM, a cantilever with a high quality (Q) factor is driven to oscillate at its eigenfrequency by positive feedback with an electronic circuit that keeps the amplitude A constant.

A cantilever with a stiffness k and effective mass m has an eigenfrequency given by $f_0 = 1/(2\pi)\,(k/m)^{1/2}$. When the cantilever is exposed to a tip-sample force gradient k_{ts}, its frequency changes instantly to $f = f_0 + \Delta f = 1/(2\pi)\,(k'/m)^{1/2}$, where $k' = k + k_{ts}$ (Fig. 2). When k_{ts} is small compared to k, the square root can be expanded and the frequency shift is
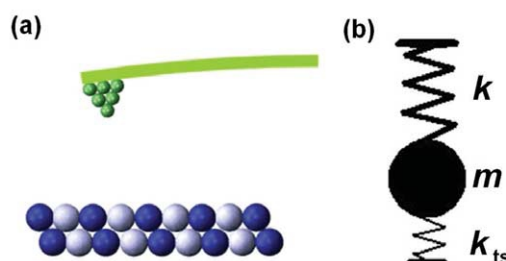

Fig. 2 (a) Schematic of a vibrating tip close to a sample in a dynamic AFM. The tip-sample forces F_{ts} cause a detectable change in the oscillation properties of the cantilever. (b) Mechanical equivalent of (a). The free cantilever with stiffness k and effective mass m has an eigenfrequency $f_0 = (k/m)^{1/2}/2\pi$. The bond between tip and sample with stiffness k_{ts} alters the resonance frequency to $f = ([k + k_{ts}]/m)^{1/2}/2\pi$. When the oscillation amplitude of the cantilever is large, k_{ts} can vary significantly within one oscillation cycle, requiring averaging.

simply given by[20]:

$$\Delta f(z) = \frac{f_0}{2k} k_{ts}(z). \tag{1}$$

This formula is only correct if k_{ts} is constant over the distance range from $z - A$ to $z + A$ that is covered by the oscillating cantilever.

The force gradient k_{ts} was probably almost constant within the oscillation interval in the first application of FM-AFM in magnetic force microscopy by Albrecht *et al.*[20], where recording media with magnetic transitions spaced by ~2 μm were imaged using a cantilever with a stiffness of ~10 N/m oscillating at an amplitude of ~5 nm. In contrast, in the more recent application of FM-AFM in atomic-resolution AFM, k_{ts} varies by orders of magnitude throughout the oscillation of the cantilever. Using FM-AFM, true atomic resolution on Si(111)-(7×7), a fairly reactive sample, was achieved in 1994[23]. Fig. 3 shows the topographic image of this data, where the fast-scanning direction is horizontal. The atomic contrast is rather poor in the lower section, quite good in a
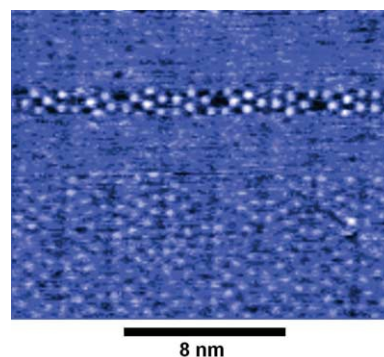

8 nm

Fig. 3 First AFM image of a reactive surface showing true atomic resolution: Si(111)-(7×7) reconstruction. Parameters: k = 17 N/m; A = 34 nm; f_0 = 114 kHz; Δf = -70 Hz; Q = 28 000; and scanning speed = 3.2 lines/s. Environment: ultrahigh vacuum, room temperature. (Reprinted with permission from[23]. © 1995 AAAS.)
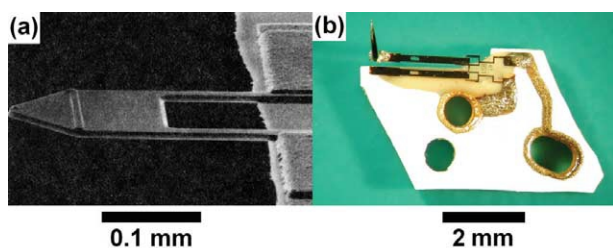
Fig. 4 Micrographs of (a) a piezoresistive cantilever[24] and (b) a 'qPlus' sensor[46] – a cantilever made from a quartz tuning fork. The piezoresistive cantilever is 250 µm long, 50 µm wide, and 4 µm thick. The eigenfrequency is 114 kHz, the stiffness 17 N/m, and the Q factor in vacuum 28 000. The qPlus sensor has a typical eigenfrequency ranging from 10-30 kHz (depending on the mass of the tip), a stiffness of 1800 N/m, and a Q factor of 4000 in vacuum at T = 300K and 20 000 at T = 4K. One of the prongs is fixed to a large substrate and a tip is mounted to the free prong. Because the fixed prong is attached to a heavy mass, the device is mechanically equivalent to a traditional cantilever. The free prong is 2.4 mm long, 130 µm wide, and 214 µm thick.

narrow strip in the center, and vanishing in the top section. These changes in contrast are the result of tip changes, indicating fairly strong interaction during the imaging process. A piezoresistive cantilever made of Si[24], as shown in Fig. 4a, with a stiffness of 17 N/m was used to obtain this image. The amplitude of the cantilever can be freely adjusted by the operator and, while it was planned to use the thermally excited amplitude[25] (~10 pm), the empirically determined optimal amplitude values were always around 10 nm – a similar order of magnitude as the value of A = 34 nm used in Fig. 3. The chemical bonding forces that are responsible for the atomic contrast in AFM imaging of Si have a range on the order of 100 pm[26], so the amplitude is 340 times as large.

The requirement of such a large amplitude is in stark contrast to intuition. Imagine an atom magnified to a size of an orange with a diameter of 8 cm. The range of the bonding force is then only 4 cm or so. The front atom of the cantilever approaches from a distance of 20 m and only in the last few centimeters of its oscillation cycle does it feel the attractive bonding forces from the sample atom next to it. On the other hand, force gradients can be quite large in chemical bonds. According to the well-known Stillinger-Weber potential[27], a single bond between two Si atoms has a force gradient of $k_{ts} \approx +170$ N/m at the equilibrium distance of $z = 235$ pm and $k_{ts} \approx -120$ N/m when the two Si atoms are at a distance of $z = 335$ pm. Because of the relatively large values of interatomic force gradients, even cantilevers with a stiffness on the order of 1 kN/m should be subject to significant frequency shifts when oscillating at small amplitudes[28]. Nevertheless, the large-amplitude FM-AFM technique has celebrated great successes in imaging

metals, semiconductors, and insulators with true atomic resolution[29-33].

Optimal imaging parameters

In order to understand why these large oscillation amplitudes are necessary, a quantitative analysis of the physics of large-amplitude FM-AFM is necessary, starting with a calculation of frequency shift for large amplitudes. If k_{ts} is not constant over one oscillation cycle, eq 1 no longer holds and a perturbation theory, such as the Hamilton-Jacobi theory[34], can be used to find the relationship between frequency and tip-sample forces[22]. Other perturbative approaches have confirmed the result[35-38], and an instructive representation of the formula is:

$$\Delta f(z) = \frac{f_0}{\pi k} \int_{-1}^{1} k_{ts}(z - uA)\sqrt{1 - u^2}\,du. \tag{2}$$

This equation is key to a physical understanding of FM-AFM, allowing evaluation of the impact of various force components on Δf, the experimental observable. At first glance, the large-amplitude result resembles eq 1, where $k_{ts}(z)$ is replaced by an averaged value. The average force gradient is computed by convoluting $k_{ts}(z)$ in the interval $z - A$ to $z + A$ with a semispherical weight function. The weight function has its maximum at $u = 0$, a distance A away from the minimal tip-sample distance. The minimal tip-sample distance z_{min} is an important parameter in any STM or AFM experiment because, while a small value of z_{min} is desirable for optimal spatial resolution, both tip and sample can be damaged if z_{min} is too small. We can now ask, if we keep z_{min} constant and vary A, what happens to our signal, the frequency shift Δf? The answer is given in eq 2: as long as the gradient of the tip-sample interaction k_{ts} remains constant as the tip of the cantilever moves over a z-range from z_{min} to $z_{min} + 2A$, Δf stays constant. However, as A reaches the decay length λ of the interaction, the frequency shift drops sharply at a rate $\propto (\lambda/A)^{3/2}$. It turns out[39] that, for amplitudes larger than λ, Δf is no longer proportional to the force gradient, but to the product of force and the square root of λ (or, equivalently, to the geometric average between potential and force[40]). In FM-AFM with amplitudes large compared to the interaction range, it is useful to define a quantity[22] $\gamma = \Delta f k A^{3/2}/f_0$. The 'normalized frequency shift' γ connects the physical observable Δf and the underlying forces F_{ts} with range λ, where $\gamma \approx 0.4 F_{ts}\lambda^{1/2}$ (see eqs 35-41 in[33]). For covalent bonds, the typical bonding strength is on the

order of -1 nN with $\lambda \approx 1$ Å, resulting in $\gamma \approx -4$ fNm$^{1/2}$, where a negative sign indicates attractive interaction. The crossover from the small-amplitude approximation in eq 1 to the large-amplitude case in eq 2 occurs for amplitudes on the order of the interaction range λ.

Eq 2 determines the influence of the oscillation amplitude on the third AFM challenge: the disturbing contribution of long-range forces. Imagine an AFM tip at a minimal distance $z_{min} = 0.3$ nm from a surface, where the total tip-sample force is composed of a chemical bonding force with an exponential distance dependence and a given range, plus a long-range force with the same strength and a ten times longer range (see Table 1 for details). In large-amplitude AFM (here, $A > 1$ nm), the signal is proportional to γ, and the long-range contribution to Δf is (1 nm/100 pm)$^{1/2}$, or approximately three times larger than the short-range contribution. For small amplitudes (here, A < 100 pm), Δf is proportional to the force gradient and the long-range component is only 100 pm/1 nm, or 1/10 of the short-range contribution. Therefore, small-amplitude AFM helps to reduce the unwanted contribution of long-range forces.

Even stronger attenuation of the unwanted long-range contribution would be possible if higher-order force derivatives could be mapped directly. For example, if we could directly measure $\partial^2 F_{ts}/\partial z^2$, the long-range component would be only 1/100 of the short-range contribution. For a direct mapping of the third-order gradient $\partial^3 F_{ts}/\partial z^3$, the relative long-range component would reduce to a mere 1/1000. Higher force gradients can be mapped directly by higher harmonic AFM, as described below.

Because the forces that act in AFM are small, optimizing the signal-to-noise ratio is crucial for obtaining good images. Frequency noise in FM-AFM is inversely proportional to amplitude[19,20,33,41]. As discussed above, the signal stays constant until A reaches λ and drops proportional to $(\lambda/A)^{3/2}$

for larger amplitudes. Therefore, the signal-to-noise ratio is maximal for amplitudes on the order of the decay length of the interaction that is used for imaging[42]. For atomic imaging, amplitudes on the order of 100 pm are expected to be optimal. As a conclusion of these calculations, we find that the use of small amplitudes $A \approx \lambda$ would have two advantages: (i) increased signal-to-noise ratio[42]; and (ii) greater sensitivity to short-range forces[33].

So, why was it not feasible to use small amplitudes in the initial experiments? Two reasons, related to the mechanical stability of the oscillating cantilever, can be identified. First, jump-to-contact is prevented if the withdrawing force of the cantilever when it is closest to the sample given by $k \times A$ is larger than the maximal attraction[22]. Second, because tip-sample forces are not conservative[43], random dissipative phenomena with a magnitude of δE_{ts} cause amplitude fluctuations[42,44] $\delta A = \delta E_{ts}/(kA)$. Both problems can be resolved by using cantilevers with sufficient stiffness. Stability considerations propose a lower threshold for k that depends on the tip-sample dissipation as well as the Q factor of the cantilever. Because the frequency shift is inversely proportional to the stiffness (eqs 1 and 2), k should still be as low as permitted by the stability requirements.

Stiff cantilevers were not available when we realized their potential advantages; therefore, we built cantilevers with a stiffness of $k = 1800$ N/m from quartz tuning forks[44-46] (Fig. 4b). A secondary advantage of quartz cantilevers is their greater frequency stability with temperature, which leads to lower frequency drift, particularly if a quartz-stabilized frequency detector is used (we used the EasyPLL by Nanosurf®, Switzerland). Other small-amplitude approaches with stiff, home-built W cantilevers have been demonstrated by the Erlandsson[47] and Pethica[48-50] groups.

As predicted by theoretical considerations, the stiff cantilever allows use of subnanometer amplitudes, resulting

Table 1 *Short- and long-range contributions to AFM signals in different operating modes.*

AFM method	Physical observable	Short-range contribution	Long-range contribution	Relative short-range contribution
Quasistatic	force	1 nN	1 nN	50%
Large-amplitude FM	$\gamma \approx 0.4 \times$ force $\times \sqrt{\text{range}}$	4 fNm$^{1/2}$	12 fNm$^{1/2}$	25%
Small-amplitude FM	force gradient	10 N/m	1 N/m	91%
Higher-harmonic	n^{th} force gradient	$10^{n+9(n-1)}$ N/m^n	$10^{9(n-1)}$ N/m^n	$\approx 100\%(1-10^{-n})$

This model calculation assumes a chemical bonding force $F(z) = F_0 e^{-z/\lambda}$ with a strength $F_{short\ range}(z_{min}) = 1$ nN and range $\lambda_{short\ range} = 100$ pm, as well as an equally strong long-range background force with $F_{long\ range}(z_{min}) = 1$ nN and a range of $\lambda_{long\ range} = 1$ nm. Depending on the mode of AFM operation, the short-range part has a different weight in the total interaction signal. Higher-harmonic AFM offers the greatest attenuation of long-range forces.
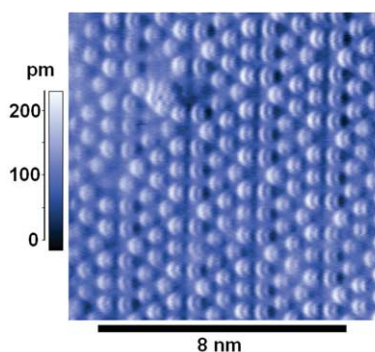
Fig. 5 AFM image of the Si 7×7 reconstruction with true atomic resolution using a stiff cantilever. Parameters: k = 1800 N/m; A = 0.8 nm; f_0 = 16.86 kHz; Δf = -160 Hz; and Q = 4000. Environment: ultrahigh vacuum, room temperature. (Reprinted with permission from[51]. © 2000 AAAS.)

Fig. 6 (a) Dynamic STM image of the Si 7×7 reconstruction using a Co_6Fe_3Sm tip mounted on a qPlus sensor. Parameters: k = 1800 N/m; A = 0.5 nm, f_0 = 19 621 Hz; sample bias voltage = -100 mV; and average tunneling current = 200 pA. Environment: ultrahigh vacuum, room temperature. (b) Schematic of tip and sample states that can lead to the experimental image shown in (a). The sample state is a dangling bond of a Si adatom with $3sp^3$ symmetry, while a Sm $4f_{z_3}$ state is taken as the tip state. (Reprinted with permission from[55,56]. © 2003 American Physical Society.)

in an improved signal-to-noise ratio, strong attenuation of long-range forces, and stable scanning at very small tip-sample distances. For these reasons, spatial resolution is increased, as shown in Fig. 5. The image shows a very clear picture of Si with a defect and very large corrugation. The adatoms of Si, which should be spherically symmetric, show subatomic details that are interpreted as orbitals in the tip atom[51,52]. This AFM image seems to show greater resolution than what was known from STM. According to the 'Stoll formula'[53], a theoretical estimate of the vertical corrugation and, thus, the lateral resolution of STM images, two physical parameters are crucial for the high spatial resolution of STM: (i) the very short decay length of the tunneling current; and (ii) a small tip-sample distance. Three likely reasons have been identified that may explain why dynamic AFM might provide better resolution than STM[54]:

- In dynamic AFM, the minimal tip-sample distance can be much smaller than in STM without destroying the tip because the shear forces that act on the front atom during scanning are much smaller in the oscillation phase where the tip is far from the sample.
- When using large gap voltages, a variety of states can contribute to the tunneling current, smearing the image.
- Tip-sample forces also have repulsive components with a very short decay length.

The first two characteristics can also be fulfilled in STM by using a very small tunneling bias voltage and oscillating the STM tip. Fig. 6 shows an image of Si obtained using dynamic STM, where a Co_6Fe_3Sm magnetic tip was mounted onto a qPlus sensor[55,56]. Each Si adatom looks like a fried egg with a sharp central peak surrounded by a halo. The radius of the central peak is only on the order of 100 pm, showing that
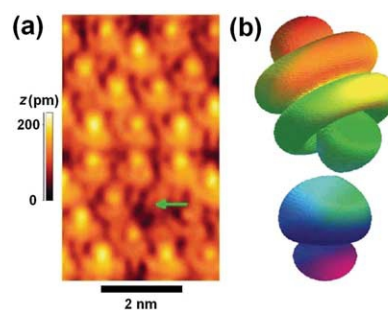
higher-momentum states[57] must have been involved in this image. The experiment was repeated with pure Co, Fe, and Sm tips, and only pure Sm tips yielded similar images to Fig. 6. We conclude, therefore, that a Sm atom acts as the tip atom in this experiment[55]. In atomic Sm, the electrons in the highest occupied state are in a $4f$ state. If one assumes that the electronic states at a Sm surface atom of bulk Co_6Fe_3Sm are similar to atomic states in Sm, it appears likely that the crystal field around the front atom creates a state close to $4f_{z_3}$ symmetry that is responsible for the tunneling contrast. Interestingly, very small tip-sample distances can only be realized with oscillating tips. When the oscillation is turned off, the current setpoint has to be reduced, otherwise the tip would not survive the small tunneling distances.

Operation at small oscillation amplitudes not only results in greater resolution, it also facilitates simultaneous STM and AFM imaging. A straightforward implementation of combined current and force measurements uses the constant-height mode, where the z-position of the tip is held constant relative to the plane connecting the surface atoms. A simultaneous measurement of tunneling current and frequency shift allows comparison of the forces and tunneling currents. Fig. 7 shows the current and repulsive force on graphite[58] observed by simultaneous AFM and STM in vacuum at liquid helium temperatures (4.9 K). STM only sees the electrons at the Fermi level, while repulsive forces act wherever the local charge density is high (i.e. over every atom) for small enough distances. In graphite, only every second surface atom conducts electricity, but every surface atom exerts repulsive forces. Therefore, AFM 'sees more' than STM and allows correlation of topography with local
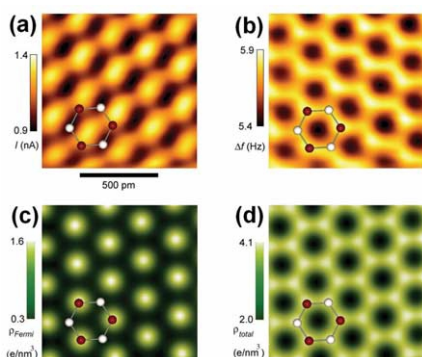
Fig. 7 (a) Constant-height STM image of graphite, and (b) simultaneously recorded AFM image (repulsive). (c) Estimate of the charge density at the Fermi level (visible in STM), and (d) total charge density (relevant for repulsive AFM) for graphite. Parameters: k = 1800 N/m; A = 0.3 nm; f_0 = 18 076.5 Hz; and Q = 20 000. (Reprinted with permission from[58]. © 2003 National Academy of Sciences, USA.)

conductance. This method is promising for other materials with more than one basis atom in the elementary cell[59,60].

While a strong bias dependence holds for atomic-resolution STM[61] as well as AFM images[60,62], a pronounced difference is that the tunneling current direction is not accessible in STM, while the measured force direction is determined by the cantilever's orientation. Usually, AFM senses forces normal to the surface, but it is also possible to perform lateral force microscopy[63] by measuring forces parallel to the surface. In a quasistatic mode, lateral forces can be recorded simultaneously with normal forces. In dynamic modes, it is easier to rotate the attachment of the cantilever by 90° and detect lateral forces. Fig. 8 shows a measurement of lateral force gradients between a tip and a Si surface. Parallel motion between tip and cantilever also allows the use of extremely soft cantilevers to probe the limits of force resolution without suffering jump-to-contact, as shown by Rugar *et al.*[64] in single-spin detection by magnetic resonance force microscopy.
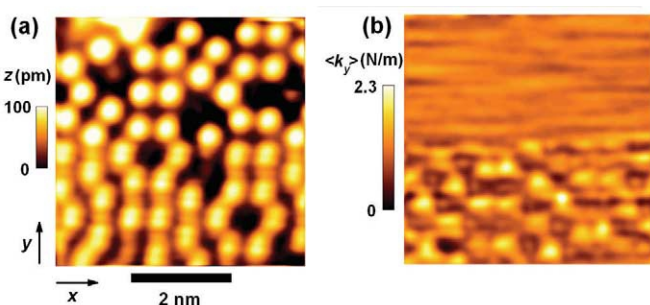

Fig. 8 (a) Topographic STM image of Si(111)-(7×7) where the tip is mounted on a lateral force sensor. The tip oscillates with $A \approx$ 80 pm in the y-direction in the lower half of the image; the oscillation is turned off in the upper half. (b) Corresponding lateral force gradient. On top of the adatoms, the bond between tip and sample causes an increase in frequency shift. Parameters: k = 1350 N/m; A = 80 pm (bottom), A = 0 (top); f_0 = 10 214 Hz. Environment: ultrahigh vacuum, room temperature[56].

Higher-harmonic AFM

Can we increase the spatial resolution of AFM any further? When decreasing the amplitude from $A >> \lambda$ to $A << \lambda$, the frequency shift changes from a proportionality of $F_{ts}\lambda^{1/2}$ to F_{ts}/λ. As outlined above, an experimental observable that is proportional to a higher force gradient should allow even higher spatial resolution than small-amplitude FM-AFM. Luckily, there is a physical observable that couples directly to higher force gradients. When the cantilever oscillates in the force field of the sample, a shift in frequency is not the only change in the cantilever's motions. The oscillation of the cantilever changes from a purely sinusoidal motion, given by $q' = A\cos(2\pi ft)$, to an oscillation that contains higher harmonics with $q' = \sum_{n=0}^{\infty} a_n\cos(2\pi nft + \phi_n)$. For amplitudes that are large with respect to the range of F_{ts}, the higher harmonics are essentially proportional[37] to Δf. However, for small amplitudes, Dürig[65] has found that F_{ts} can be recovered immediately within the distance range from z_{min} to z_{min} + 2A if the amplitudes and phases of all higher harmonics of the cantilever's motion are known. Moreover, higher harmonics bear even more useful information: direct coupling to higher force gradients[66]. Similar to eq 2, we can express the magnitude of the higher harmonics by a weighted average of a force gradient – a gradient of order $n > 1$ this time:

$$a_n = \frac{2}{\pi k}\frac{1}{1-n^2}\frac{A^n}{1 \cdot 3 \cdot \ldots \cdot (2n-1)}\int_{-1}^{1}\frac{d^n F_{ts}(z+Au)}{dz^n}(1-u^2)^{n-1/2}du. \quad (3)$$

The weight function changes from the semispherical shape $w_{\Delta f}(u) = (1 - u^2)^{1/2}$ in eq 2 to functions $w_n(u) = (1 - u^2)^{n-1/2}$ that are more and more peaked with increasing n. For this reason, the use of small amplitudes is of even greater importance in higher harmonic AFM than in FM-AFM. The magnitude of the higher harmonic amplitudes a_n is rather small compared to the fundamental amplitude $a_1 = A$; therefore, higher harmonic AFM works best at low temperatures, where the detection bandwidth can be set to very small values.

The spatial resolution of AFM and STM is fundamentally limited neither by the mechanical vibration level nor by thermal vibrations, but by the spatial extent of the experimental objects that are observed – electrons at the Fermi level in STM[67] and something close to the total charge density in repulsive AFM[68]. When probing the resolution limits of AFM, we first have to find an object with the desired sharply localized electronic states. Pauling[69] noted that
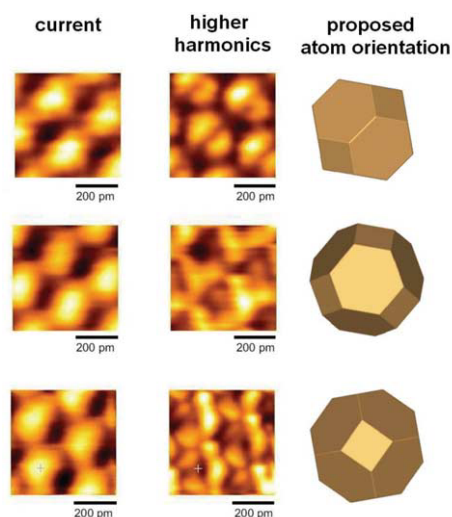
Fig. 9 Simultaneous constant-height STM (left column) and higher-harmonic AFM images (central column) of graphite using a W tip. The right column shows the proposed orientation of the W tip atom. The W atom is represented by its Wigner-Seitz unit cell, which reflects the full symmetry of the bulk. We assume that the bonding symmetry of the adatom is similar to the bonding symmetry of the bulk. This assumption is based on charge density calculations of surface atoms[70,71]. In the first row, the higher harmonics show a two-fold symmetry, resulting from a [110] orientation of the front atom. In the second row, the higher harmonics show a roughly three-fold symmetry, as expected for a [111] orientation. In the third row, the symmetry of the higher-harmonic signal is approximately four-fold, as expected for a tip in [001] orientation. Parameters: $k = 1800$ N/m; $A = 0.3$ nm; $f_0 = 18\,076.5$ Hz; and $Q = 20\,000$. Environment: ultrahigh vacuum, $T = 4.9$ K. (Reprinted with permission from[66]. © 2004 AAAS.)

transition metals show a covalent bonding character and should therefore expose lobes of increased charge density toward their neighbors. Indeed, while the surface atoms of W(001) expose a large blurred charge cloud at the Fermi level for k-vectors perpendicular to the surface (Fig. 8 in[70]), the total charge density shows four distinct maxima (Fig. 3 in[70] and Fig. 3a in[71]). Fig. 9 shows a direct comparison of the simultaneously recorded tunneling current and higher harmonic amplitudes. As expected, the higher harmonic data shows much greater detail.

Summary and conclusion

We have substantiated the enormous usefulness of AFM by referring to the numerous references to the original publication[2] in the introduction. While most AFM applications are currently not in the atomic-resolution regime, the enhancement in spatial resolution is likely to create value in most AFM studies in physics, chemistry, biology, and materials science.

Recently, true atomic resolution in FM-AFM has been observed at ambient pressure in an N_2 atmosphere[72], showing that some of the concepts of vacuum AFM are applicable in ambient environments. Although STM resolution
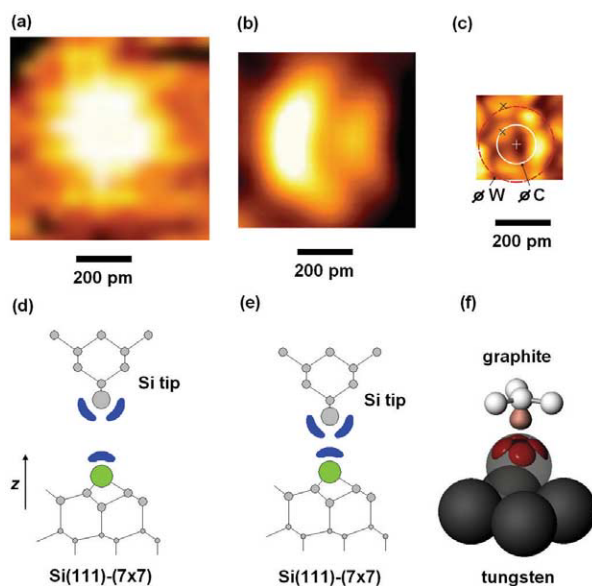

Fig. 10 Progress in AFM spatial resolution showing images of single atoms. The lateral scale in (a)-(c) is equal. (a) An adatom of the Si(111)-(7×7) reconstruction, showing up as a blurred spot. (b) An adatom of the Si(111)-(7×7) reconstruction, showing subatomic contrast originating in the electronic structure of the tip. (c) Higher-harmonic image of a W atom mapped by a carbon atom. Parameters: (a) $k = 17$ N/m; $A = 34$ nm; $f_0 = 114$ kHz, $\Delta f = -70$ Hz; and $Q = 28\,000$ (ultrahigh vacuum, room temperature); (b) $k = 1800$ N/m; $A = 0.8$ nm; $f_0 = 16\,860$ Hz; $\Delta f = -160$ Hz; and $Q = 4\,000$ (ultrahigh vacuum, room temperature); (c) $k = 1800$ N/m; $A = 0.3$ nm; $f_0 = 18\,076.5$ Hz; and $Q = 20\,000$ (ultrahigh vacuum, $T = 4.9$ K), higher harmonic detection. (d) Schematic of a Si(001) tip close to a Si(111)-(7×7) surface. Because of the large amplitude and a fairly large minimum tip-sample distance, the blurry image (a) corresponding to this configuration is approximately symmetric with respect to the vertical axis. (e) Similar to (d), but at a closer distance. The angular dependence of the bonding forces is noticeable. (f) W(001) surface close to a carbon atom in a graphite surface. The charge distribution in W shows small pockets that are resolved by higher-harmonic AFM with a light-atom carbon-probe. (Parts (c) and (f) reprinted with permission from[66]. © 2004 AAAS.)

can benefit from oscillating the tip, a concept that originated in AFM, Fig. 9 shows that AFM has now clearly reached and even surpassed the resolution capability of STM. Fig. 10 shows the evolution of AFM resolution from large-amplitude AFM in 1994 (Fig. 10a) to small-amplitude AFM in 2000 (Fig. 10b) and higher-harmonic AFM in 2004 (Fig. 10c). While the structures within single atoms shown in Figs. 10b and 10c originate in the front atom of the probe, there are other examples where AFM shows more atomic details than STM that establish the improved spatial resolution of AFM over STM in special cases. These include the observation of the rest atoms in Si(111)-(7×7)[73,74] or the observation of all dangling bonds on the Si/Ge(105) surface[75].

Atomic and molecular structuring has long been the domain of STM, from the first demonstration of manipulating single atoms[76] to a variety of STM nanofabrication methods[77]. Recently, it has been shown that atomic manipulation by AFM is possible even at room temperature[78].

We have not been able to discuss the phenomenal success of AFM in biology, a field with a much more immediate impact on the human condition. It can be expected that at least some of the concepts that have been developed for AFM in vacuum will enable greater resolution in biological AFM applications as well[79,80]. MT

REFERENCES

1. Binnig, G., Atomic Force Microscope and Method for Imaging Surfaces with Atomic Resolution, US Patent 4,724,318, (1986)

2. Binnig, G., *et al.*, *Phys. Rev. Lett.* (1986) **56** (9), 930

3. Binnig, G., and Rohrer, H., *Rev. Mod. Phys.* (1999) **71** (2), S324

4. Faraday, M., *Chemical History of a Candle,* Dover Publications, Mineola, NY, (2003)

5. Siegman, A. E., *Lasers,* University Science Books, Herndon, VA, (1986)

6. Binnig, G., *et al.*, *Phys. Rev. Lett.* (1982) **49** (1), 57

7. Hofer, W. A., *Materials Today* (2002) **5** (10), 24

8. Binnig, G., *et al.*, *Phys. Rev. Lett.* (1983) **50** (2), 120

9. Takayanagi, K., *et al.*, *J. Vac. Sci. Technol. A* (1985) **3** (3), 1502

10. Binnig, G., *et al.*, *Europhys. Lett.* (1987) **3**, 1281

11. Albrecht, T. R., and Quate, C. F., *J. Appl. Phys.* (1987) **62** (7), 2599

12. Meyer, G., and Amer, N. M., *Appl. Phys. Lett.* (1990) **56** (21), 2100

13. Meyer, E., *et al.*, *Z. Phys. B: Condens. Matter* (1990) **79**, 3

14. Riordon, J., *APS News* (2003) May, 3

15. Rugar, D., and Hansma, P., *Phys. Today* (1990) **43**, 23

16. Giessibl, F. J., and Binnig, G., *Ultramicroscopy* (1992) **42-44** (1), 281

17. Ohnesorge, F., and Binnig, G., *Science* (1993) **260**, 1451

18. Howald, L., *et al.*, *Phys. Rev. B* (1995) **51** (8), 5484

19. Martin, Y., *et al.*, *J. Appl. Phys.* (1987) **61** (10), 4723

20. Albrecht, T. R., *et al.*, *J. Appl. Phys.* (1991) **69** (2), 668

21. Dürig, U., *et al.*, *J. Appl. Phys.* (1992) **72** (5), 1778

22. Giessibl, F. J., *Phys. Rev. B* (1997) **56** (24), 16010

23. Giessibl, F. J., *Science* (1995) **267**, 68

24. Tortonese, M., *et al.*, *Appl. Phys. Lett.* (1993) **62**, 834

25. Giessibl, F. J., *Jpn. J. Appl. Phys., Part 1* (1994) **33** (6B), 3726

26. Perez, R., *et al.*, *Phys. Rev. Lett.* (1997) **78** (4), 678

27. Stillinger, F. H., and Weber, T. A., *Phys. Rev. B* (1985) **31** (8), 5262

28. Giessibl, F. J., German Patentschrift DE 196 33 546, (1996)

29. Morita, S., *et al.* (eds.), *Noncontact Atomic Force Microscopy*, Springer, Berlin, (2002)

30. Meyer, E., *et al.*, *Scanning Probe Microscopy: The Lab on a Tip*, Springer, Berlin, (2003)

31. Garcia, R., and Perez, R., *Surf. Sci. Rep.* (2002) **47** (6-8), 197

32. Hofer, W. A., *et al.*, *Rev. Mod. Phys.* (2003) **75**, 1287

33. Giessibl, F. J., *Rev. Mod. Phys.* (2003) **75**, 949

34. Goldstein, H., *Classical Mechanics*, Addison Wesley, Reading, MA (1980)

35. Baratoff, A., unpublished results (1997)

36. Dürig, U., *Surf. Interface Anal.* (1999) **27** (5-6), 467

37. Dürig, U., *Appl. Phys. Lett.* (1999) **75** (3), 433

38. Livshits, A. I., *et al.*, *Appl. Surf. Sci.* (1999) **140** (3-4), 327

39. Giessibl, F. J., and Bielefeldt, H., *Phys. Rev. B* (2000) **61** (15), 9968

40. Ke, S. H., *et al.*, *Phys. Rev. B* (1999) **59** (20), 13267

41. Hasegawa, Y., *et al.*, *Jpn. J. Appl. Phys.* (2004) **43** (2B), L303

42. Giessibl, F. J., *et al.*, *Appl. Surf. Sci.* (1999) **140** (3-4), 352

43. Kantorovich, L. N., *Phys. Rev. B* (2001) **64** (24), 245409

44. Giessibl, F. J., *et al.*, *Nanotechnology* (2004) **15** (2), S79

45. Giessibl, F. J., *Appl. Phys. Lett.* (1998) **73** (26), 3956

46. Giessibl, F. J., *Appl. Phys. Lett.* (2000) **76** (11), 1470

47. Erlandsson, R., *et al.*, *Phys. Rev. B* (1997) **54** (12), R8309

48. Hoffmann, P. M., *et al.*, *Proc. R. Soc. London, Ser. A* (2001) **457**, 1161

49. Hoffmann, P. M., *et al.*, *Phys. Rev. Lett.* (2001) **87** (26), 265502

50. Oral, A., *et al.*, *Appl. Phys. Lett.* (2001) **79** (12), 1915

51. Giessibl, F. J., *et al.*, *Science* (2000) **289**, 422

52. Huang, M., *et al.*, *Phys. Rev. Lett.* (2003) **90**, 256101

53. Stoll, E., *Surf. Sci. Lett.* (1984) **143** (2-3), L411

54. Giessibl, F. J., *et al.*, *Ann. Phys. (Leipzig)* (2001) **10** (11-12), 887

55. Herz, M., *et al.*, *Phys. Rev. B* (2003) **68**, 045301

56. Herz, M., Dynamische Tunnel-, Kraft- und Reibungsmikroskopie mit atomarer und subatomarer Auflösung, PhD thesis, University of Augsburg, Germany, (2003), www.lob.de

57. Chen, C. J., *Introduction to Scanning Tunneling Microscopy*, Oxford University Press, New York, (1993)

58. Hembacher, S., *et al.*, *Proc. Natl. Acad. Sci. USA* (2003) **100** (22), 12539

59. Hembacher, S. F., Simultane Rasterkraft- und Rastertunnelmikroskopie bei 5 K im Ultrahochvakuum, PhD thesis, University of Augsburg, Germany, (2003), www.dissertation.de

60. Hembacher, S., *et al.*, *Phys. Rev. Lett.* (2005) **94**, 056101

61. Feenstra, R. M., *et al.*, *Phys. Rev. Lett.* (1987) **58** (12), 1192

62. Arai, T., and Tomitori, M., *Phys. Rev. Lett.* (2004) **93**, 256101

63. Mate, C. M., *et al.*, *Phys. Rev. Lett.* (1987) **59** (17), 1942

64. Rugar, D., *et al.*, *Nature* (2004) **430**, 329

65. Dürig, U., *New J. Phys.* (2000) **2**, 5

66. Hembacher, S., *et al.*, *Science* (2004) **305**, 380

67. Tersoff, J., and Hamann, D. R., *Phys. Rev. Lett.* (1985) **50** (25), 1998

68. Ciraci, S., *et al.*, *Phys. Rev. B* (1990) **41** (5), 2763

69. Pauling, L., *The Nature of the Chemical Bond*, Cornell University Press, Ithaca, NY, (1957)

70. Posternak, M., *et al.*, *Phys. Rev. B* (1980) **21** (12), 5601

71. Mattheiss, L. F., and Hamann, D. R., *Phys. Rev. B* (1984) **29** (10), 5372

72. Sasahara, A., *et al.*, *J. Phys. Chem. B* (2004) **108** (40), 15735

73. Lantz, M. A., *et al.*, *Phys. Rev. Lett.* (2000) **84** (12), 2642

74. Eguchi, T., and Hasegawa, Y., *Phys. Rev. Lett.* (2002) **89**, 266105

75. Eguchi, T., *et al.*, *Phys. Rev. Lett.* (2004) **93**, 266102

76. Eigler, D. M., and Schweizer, E. K., *Nature* (1990) **344**, 524

77. Rosei, F., *J. Phys.: Condens. Matter* (2004) **16** (17), S1373

78. Sugimoto, Y., *et al.*, *Nat. Mater.* (2005) **4** (2), 156

79. Miles, M., *Science* (1997) **277**, 1845

80. Hörber, J. K. H., and Miles, M. J., *Science* (2003) **302**, 1002